Nanoscale patterning of chemical order induced by displacement cascades in irradiated alloys. II. Analytical modeling

Jia Ye and Pascal Bellon*
Department of Materials Science and Engineering, University of Illinois at Urbana-Champaign, Illinois 61801, USA
(Received 19 February 2004; published 8 September 2004)

We study analytically the effect of the chemical disorder produced by displacement cascades in a stoichiometric $L1_2$ alloy under irradiation. A continuum kinetic model is proposed to describe the coupled evolution under irradiation of the specific area covered by antiphase boundaries and of the volume fraction of the domains belonging to the four translation variants of the $L1_2$ structure. Combining this description with existing mean-field results for the order-disorder transition under irradiation, we construct a steady-state dynamical phase diagram, where the control parameters are the cascade size and the irradiation-induced disordering rate. Three stable steady states are predicted: long-range ordered, disordered, and a state of patterning of order. This analytical phase diagram is in good agreement with the one constructed from kinetic Monte Carlo simulations. The present analytical model indicates that patterning of chemical order should be a general phenomenon in irradiated ordered structures, provided that the cascade size is large enough for the annealing of disordered zones to form additional antiphase domains.

DOI: 10.1103/PhysRevB.70.094105 PACS number(s): 61.80.Az, 05.70.Ln, 47.54.+r, 64.60.Cn

I. INTRODUCTION

In a previous paper,[1] hereafter referred to as Part 1, we have employed kinetic Monte Carlo (KMC) simulations to study the evolution and the steady-state properties of the field of chemical order in a binary alloy subjected to sustained irradiation. The irradiation conditions are chosen such that they lead to the formation of dense displacement cascades, and thus to the introduction of disordered zones. These disordered zones result from forced atomic mixing in the cascades, and the size and the degree of disordering vary with the mass and energy of the irradiation projectile. As reviewed in Part 1,[1] disordered zones have been characterized experimentally using dark-field transmission electron microscopy (DF-TEM) imaging, and specific details of the disorder produced by energetic cascades have been investigated by molecular dynamics (MD) simulations. The important points in the context of this work is that cascade sizes range from a few to about ten nanometers, and that the cascade destroys any preexisting long-range order (LRO), while some short range order (SRO) may form during the cooling phase of the cascade.

For the $L1_2$ model binary alloy studied in Part 1, at the stoichiometric composition A_3B, three stable microstructures of order are identified under steady-state conditions: long-range ordered, disordered with some SRO, and patterns of order. The last microstructure is comprised of well-ordered domains with a finite average size, and these domains belong in equal proportions to the four translation variants of the $L1_2$ structure. In contrast, the LRO state contains only one macroscopic variant. The dynamical stability of the three steady states is determined by three irradiation parameters, namely the irradiation temperature, the number of pairs of atom exchanged in a cascade, b, and the cascade introduction rate Γ_c, or equivalently the ballistic pair exchange frequency, $\Gamma_b = b \times \Gamma_b$. In the results reported in Part 1, simulations were performed at constant temperature, and a dynamical phase diagram was built, which yields the domain of stability of the three steady states in the (Γ_b, b) plane. A remarkable feature of this diagram is that, for patterning of order to take place, the cascade size has to exceed a threshold value. The existence of a threshold is related to the effect of the cascade size on the reordering path of a disordered zone. For large zones, reordering proceeds in two stages. First, new ordered domains form in the disordered zone and grow until they fill the whole volume initially disordered by the cascade. These new domains then shrink and disappear by the inward motion of antiphase boundaries (APBs) that form between the surrounding matrix and these small domains. By contrast, small disordered zones are directly annealed by the inward migration of the matrix-disordered zone interface, and thus they do not lead to the formation of antiphase domains. In the absence of this key component, patterns of order are not observed at steady state in the KMC simulations.

In the present work, we derive in Secs. II and III an analytical model to study the transition from a patterning state, which lacks long-range order, to a long-range ordered state. In Sec. IV we combine these results with an ordered-disordered boundary built by applying earlier mean field results. This combination makes it possible to construct an analytical steady-state phase diagram, which is then compared to the one determined by KMC simulations in Part 1.

II. INTERFACE AND VOLUME RATE EQUATIONS IN THE ABSENCE OF IRRADIATION

Our goal in Secs. II and III is to establish a simple model that captures the proper physics to reproduce the dynamical competition between the long-range ordered state and the patterning state. In Sec. II, we first build this model in the absence of irradiation, and in Sec. III we extend this model by including irradiation contributions.

In the patterned state, the four translation variants of the $L1_2$ phase are found in equal proportions, i.e., the specific

volumes occupied by each variant are equal $V_{i,v}=1/4$ where $i=1,4$ labels the variants—note that here we neglect the volume occupied by disordered regions and by APBs. By contrast, in the long-range ordered state the microstructure is dominated by one variant. We will thus identify the transition from the patterned to the LRO state by determining the conditions where $V_{i,v}=1/4$ ceases to be a stable solution of the kinetic equations. As seen later, the specific area covered by APBs, S_v, enters the kinetic equation we derive for $V_{v,i}$. We therefore need at least two variables, $V_{i,v}$ and S_v, to characterize the order field. We will show that this description is sufficient to capture the transition from patterning to LRO, although these two variables do not specify all the characteristics of the microstructure, in particular they do not contain any direct information on the connectivity of the domains. For the sake of simplicity, we first derive the volume and interface kinetic equations for an ordered structure that possesses only two variants, e.g., the $B2$ structure in a bcc lattice. The results are then generalized to structures with more than two variants, including the $L1_2$ structure.

We first consider the rate of evolution of the area covered by APBs. This interface kinetic equation has already been derived by Allen and Cahn[2] to study domain growth during isothermal annealing. We recall here the important steps of this derivation, as we will propose a related treatment to derive the volume equation. Starting from a time-dependent Guinzburg-Landau description for the relaxation rate of the order parameter, Allen and Cahn showed that the local velocity of an APB separating the two variants of the ordered structure is proportional to a mobility, M, times the local mean curvature of the APB, K, which is defined as $K=K_1+K_2$, where K_1 and K_2 are the principal curvatures:

$$v = M(K_1 + K_2). \tag{1}$$

By convention, the mean curvature in Eq. (1) is positive when the interface is concave on the side toward which the normal to the interface is directed. Equation (1) shows that a spherical antiphase domain should shrink and disappear. A geometrical relationship is then used to relate an elemental area of APB, dS, and its change $\delta(dS)$ during a time δt:

$$\delta(dS) = -(v\,\delta t)(dS)(K_1 + K_2). \tag{2}$$

The integration of Eq. (2) and use of Eq. (1) yields a differential equation for the temporal evolution of S:

$$\frac{dS}{dt} = -M \int (K_1 + K_2)^2 dS. \tag{3}$$

Allen and Cahn introduce then an averaged squared mean curvature:

$$K_m^2 = \langle (K_1 + K_2)^2 \rangle = \frac{1}{S} \int (K_1 + K_2)^2 dS, \tag{4}$$

so that the specific area of APBs, S_v, obeys the relation

$$\frac{dS_v}{dt} = -MK_m^2 S_v. \tag{5}$$

Finally, under the assumption that the microstructure is characterized by only one length scale, S_v and K_m should be proportional to each other: $K_m^2=\phi S_v^2$. Substituting this relationship in Eq. (5), one obtains the classical Allen-Cahn equation. The integration of this equation with respect to time indicates that the change of $(S_v)^{-2}$ is linear with time. It also predicts that a spherical antiphase domain shrinks at a rate such that its interfacial area decays linearly with time. This kinetics is indeed well obeyed in our KMC simulations (see Ref. 29 in Part 1). We note that at temperatures lower than the one considered here, point defect trapping may produce long-lived transient with different exponents.[3]

We now turn to the derivation of the volume equation. Following an approach similar to the one reviewed above, a geometrical equation, analogous to Eq. (2) is obtained for the change of an infinitesimal volume of variant 2, dV_2, during a time δt:

$$\delta(dV_2) = -v\,\delta t dS = -MK\delta t dS. \tag{6}$$

By convention, the normal of the interface is chosen to point into the variant 2, and as a result, when K is positive, $\delta(dV_2)$ is negative, as expected. Integration of this equation over a macroscopic volume leads to

$$\frac{dV_2}{dt} = -M \int (K_1 + K_2) dS. \tag{7}$$

During the nucleation, growth, and coarsening of ordered domains in an isothermally annealed alloy, all variants should be found in equal proportion, until the domains reach a size where, because of finite size effects, one variant dominates the microstructure. It is therefore expected that, before the manifestation of finite size effects, the probability distribution of local mean curvatures, $p(K)$, is an even function of K. This property has indeed been observed in numerical simulations relying on a time-dependent Guinzburg-Landau (TDGL) equation.[4,5] These simulations also indicate that $p(K)$ is centered around $K=0$. The RHS of Eq. (7) can be re-expressed with $p(K)$ as $\int K dS = S \int K p(K) dK$. As long as $p(K)$ remains an even function, the integral on the right-hand side of Eq. (7) is zero, and the volume fractions of each variant do not change with time. When finite size effects become noticeable, fluctuations lead to the development of a small asymmetry in $p(K)$. This asymmetry increases with time and thus one variant grows at the expense of the other. $V_{2,v}=1/2$ should therefore be an unstable solution of Eq. (7).

In systems undergoing thermal annealing, the volume equation, Eq. (7), does not provide any new information, and the interface equation, Eq. (5), is sufficient to model the evolution of the domain microstructure. For an alloy under irradiation, we will use the volume equation to track the transition from the patterned state to the LRO state. Indeed, in the patterned state $V_{2,v}=1/2$ is a stable solution, whereas it is unstable in the LRO state, just as in a finite-size thermal system. In order to proceed further, we need to obtain an evaluation of the integral in Eq. (7) at the onset of asymmetry between the two ordered variants. This integral is difficult to evaluate, as the exact distribution $p(K,t)$ is unknown. We introduce here an approximation to evaluate this integral for a microstructure that is initially mostly symmetric, i.e., $V_{2,v} \approx 1/2$. We decompose $p(K,t)$ into a symmetric and an asym-

metric component, and we assume that the asymmetric component is infinitesimally small: $p(K)=p_+(K)+\varepsilon p_-(K)$, where $0<\varepsilon\ll 1$. We note that, since $p(K)$ is a normalized distribution, i.e., $\int p(K)dK=1$, a similar relationship holds also for $p_+(K)$ up to first order in ε; in contrast, $p_-(K)$ is not normalized and instead $\int p_-(K)dk=0$. The integral on the RHS of Eq. (7) now reads as

$$\int KdS = S\int_{-\infty}^{+\infty} Kp(K)dK = 2\varepsilon S\int_{-\infty}^{0} Kp_-(K)dK. \qquad (8)$$

Because of the statistical nature of the components $p_+(K)$ and $p_-(K)$, we now assume that, except for a sign difference, they follow a similar K-dependency:

$$p_-(K)\approx -p_+(K),\ \text{for } K<0,$$

$$p_-(K)\approx p_+(K),\ \text{for } K>0. \qquad (9)$$

In Eq. (9), by convention, we have assumed that the small asymmetry of $p(K)$ favors the positive values of K, i.e., $p_-(K)>0$ for $K>0$; this implies that the volume fraction of the variant 2 will decrease with time. The assumption leading to Eq. (9) allows us to relate the last integral in Eq. (8) for $p_-(K)$ to a similar integral, but now involving $p_+(K)$. In order to evaluate this integral, we assume without loss of generality that $p_+(K)$ follows a Gaussian distribution of zero mean and variance σ.[6] The integral in Eq. (8) can now be reevaluated:

$$\int_{-\infty}^{0} Kp_-(K)dK = -\int_{-\infty}^{0} Kp_+(K)dK = \frac{\sigma}{\sqrt{2\pi}}. \qquad (10)$$

The integral identified in the interface equation, Eq. (3), can also be calculated in terms of σ.

$$\int K^2dS = S\int_{-\infty}^{+\infty} K^2p_+(K)dK = S\sigma^2. \qquad (11)$$

By identification with Eq. (4), we have $\sigma^2=K_m^2$, and the volume equation, Eq. (7), can now be rewritten as

$$\frac{dV_2}{dt} = -2M\frac{\varepsilon S}{\sqrt{2\pi}}K_m. \qquad (12)$$

In the last equation, εS can be interpreted as the amount of interfacial area involved in the development of the asymmetry of $p(K)$. The last step is to express this quantity in terms of the excess volume of the variant two. For that purpose, let us decompose εS into a sum of area δS_i. Following the assumption made by Allen and Cahn that there is only one length scale that characterizes the microstructure, we have $\varepsilon S=\Sigma_i\delta S_i\propto\Sigma_i K_i\delta V_i$, where K_i is the local curvature and δV_i is the excess (or lack) of volume occupied by the variant two. Finally, we assume that K_i and dV_i are uncorrelated so that $\varepsilon S_v\propto K_m(1/2-V_{2,v})$. The evolution of the volume fraction of the variant two is finally given by

$$\frac{dV_{2,v}}{dt} = -C_1M\left(\frac{1}{2}-V_{2,v}\right)K_m^2 = -C_1\phi M\left(\frac{1}{2}-V_{2,v}\right)S_v^2, \qquad (13)$$

where C_1 and ϕ are positive dimensionless constants. We see that Eq. (13) has the two expected properties for an alloy undergoing annealing in the absence of irradiation: $V_{2,v}=1/2$ is always a steady-state solution, but this solution is unstable. Equation (13) thus predicts that, after a finite annealing time, a finite size system will always reach the LRO state. It is also worth mentioning that, from a dimensional analysis standpoint, the terms M and S_v^2 are expected in Eq. (13).

In the case of a structure with $N>2$ variants, the above derivation of the volume equation can be easily generalized by isolating the one variant that will grow in the latest stage of the annealing, and by recognizing that the remaining $N-1$ variants are statistically equivalent. Therefore, one only needs to focus on APBs separating the leading variant, say variant one, from any shrinking variant, say variant two, and follow step by step the above derivation given for the case $N=2$. Defining now S_v as the specific APBs area between the variants one and two, and K_m^2 as the averaged square mean curvature of these APBs, the interface and volume equations become

$$\frac{dS_v}{dt} = -M\phi S_v^3,$$

$$\frac{dV_{2,v}}{dt} = -C_2M\left(\frac{1}{N}-V_{2,v}\right)\phi S_v^2, \qquad (14)$$

where C_2 is a dimensionless positive constant. In particular in the following sections we will use these equations for the $L1_2$ structure, for which $N=4$.

III. INTERFACE AND VOLUME EQUATIONS IN THE PRESENCE OF IRRADIATION

From simple geometrical considerations, we derive in this section the contributions to the interface and volume equations of the disordered zones produced by displacement cascades. This derivation is performed under two assumptions: (i) the disordered zones are large enough for their reordering to introduce new antiphase domains, and (ii) the ballistic jump frequency is small enough so that, overall, the microstructure is well ordered and the volume covered by disordered regions is negligible. We will return to these two assumptions in Sec. IV when constructing the dynamical phase diagram. In order to facilitate the comparison with the KMC results reported in Part 1, we focus the present derivation on the $L1_2$ ordered structure, but the extension to other ordered structures is straightforward. Since the $L1_2$ structure has four translation variants, a spherical disordered zone of radius r produces on average four new domains, each occupying a quarter of the disordered volume. Furthermore, we assume for simplicity that interfaces between the four new domains are along equatorial planes of the sphere. Under these conditions, each cascade creates $6\pi r^2$ interface, of which $5\pi r^2$

corresponds to new APBs. Meanwhile, the same cascade destroys $4\pi r^3 S_v/3$ of APBs that may have existed in the sphere before the initiation of the displacement cascade. The cascade radius can be expressed in terms of the cascade size b, the cascade density −80% in our KMC simulations, and the atom density ρ:

$$0.80 \times \frac{4}{3}\pi r^3 \rho = 2b. \tag{15}$$

For a fcc crystal, the atom density is $\rho = 4/a^3$, where a is the lattice parameter. Taking into account the two above effects, we can write the interface equation with the contributions due to irradiation:

$$\frac{dS_v}{dt} = -\phi M S_v^3 + Ab^{-1/3}\Gamma_b - \rho^{-1}\Gamma_b S_v, \tag{16}$$

where $A = 5\pi(0.8 \times 4\pi\rho/3)^{-2/3}$, and Γ_b is the ballistic atom exchange frequency.

The contribution of the disordering and reordering of the cascade to the volume equation is straightforward, as each cascade, on average, destroys a volume of variant two proportional to $V_{2,v}$, and replaces it by one quarter of the cascade volume. The resulting volume equation, with both thermal and irradiation contributions, is given by

$$\frac{dV_{2,v}}{dt} = -C_2 M\left(\frac{1}{4} - V_{2,v}\right)\phi S_v^2 + \left(\frac{1}{4} - V_{2,v}\right)\rho^{-1}\Gamma_b. \tag{17}$$

IV. STEADY-STATE SOLUTIONS AND DYNAMICAL PHASE DIAGRAM

Steady-state solutions of the interface and volume equations satisfy

$$\frac{dS_v}{dt} = -\phi M S_v^3 + Ab^{-1/3}\Gamma_b - \rho^{-1}\Gamma_b S_v = 0,$$

$$\frac{dV_{2,v}}{dt} = -C_2 M\left(\frac{1}{4} - V_{2,v}\right)\phi S_v^2 + \left(\frac{1}{4} - V_{2,v}\right)\rho^{-1}\Gamma_b = 0. \tag{18}$$

From the above volume equation, we see that the solution $V_{2,v} = 1/4$ changes from stable to unstable when

$$S_v = \sqrt{\frac{\Gamma_b}{C_2 M \rho \phi}}. \tag{19}$$

Substituting Eq. (19) into the steady-state solution of the interface equation Eq. (18) yields the relationship satisfied at the patterning-LRO instability boundary:

$$b = \left(\frac{C_2 A \rho}{1 + C_2}\right)^3 \left(\frac{\Gamma_b}{C_2 M \rho \phi}\right)^{-3/2}. \tag{20}$$

We stated at the beginning of Sec. III that, for the derivation of the patterning-LRO boundary, we used two assumptions. The first one is that the cascade size is large enough for the reordering to proceed in two stages and to lead to the formation of antiphase domains. Below a certain cascade size, b_c, this assumption is no longer valid, as the reordering proceeds directly by the migration of the matrix-zone interface. Eq. (20) is thus only valid for $b \geqslant b_c$. When $b < b_c$, patterning is no longer possible, and upon increasing the ballistic exchange frequency, the LRO steady state is destabilized to the benefit of the disordered steady state. This order-disorder boundary can be calculated starting from the TDGL kinetic model used by Allen and Cahn in the derivation of Eq. (1), and extending this model by adding the disorder produced by displacement cascades. Here, in order to take advantage of specific results available in the literature, we consider instead mean-field Bragg-Williams kinetic models. In the Bragg-Williams approximation, a mean-field point approximation, correlations of atomic occupancies on lattice sites are ignored. We note that a Guinzburg-Landau or Cahn-Hilliard free-energy functional can be easily derived from a Bragg-Williams approximation.[7] In the context of our study, the main result already obtained from Bragg-Williams kinetic models for alloys under irradiation is that the instability boundary from the disordered steady state to the long-range order steady state is only a function of Γ_b.[8] This boundary corresponds thus to a vertical line in the (Γ_b, b) plane. This result is based on a Fokker-Planck approximation of the master equation that describes the temporal evolution of the distribution probability of the degree of order. This approach makes it possible to take into account the fact that the ballistic exchanges taking place during the displacement cascade are highly correlated in time.[8] The above result, which was obtained for an $A2$-$B2$ transition, is valid for other ordered phases as well, since the disorder-order instability only involves the first moment of the Fokker-Planck expansion, and this first moment is only proportional to $b \times \Gamma_c$, i.e., to Γ_b. The ballistic exchanges forced by a cascade are also strongly correlated in space, but these correlations cannot be taken into account in a point approximation.

The resulting analytical dynamical phase diagram is shown in Fig. 1. We note the existence of three regions. At high Γ_b values, the disordered state is locally stable (region labeled "D"); at lower Γ_b values and for large cascade sizes, the disordered state is unstable toward ordering, and the patterned state is locally stable (region labeled "P"); finally, at low Γ_b values and for small cascade sizes (region labeled "LRO"), the disordered state is unstable toward ordering and the patterned state is either unstable (for $b > b_c$) or not physically accessible (for $b < b_c$). We note that the second approximation used in the derivation of the patterning-LRO boundary is fulfilled: as this boundary is always to the left of the disorder-order instability line, the disordered zones produced by displacement cascades will re-order, and it was thus legitimate to ignore disordered regions in the derivation of the volume equation, Eq. (13).

V. DISCUSSION

The dynamical phase diagram constructed in Fig. 1 is based on instability boundaries. A complete determination of this phase diagram would require the construction of the global stability boundaries for the first-order transitions between

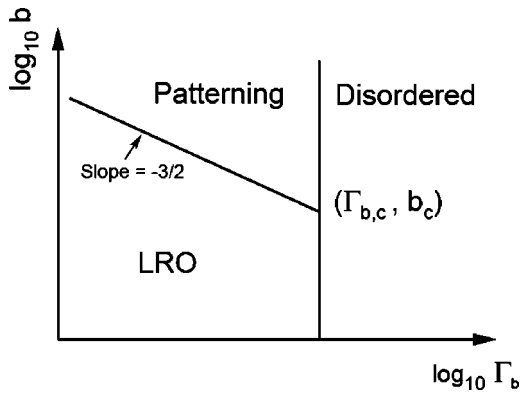

FIG. 1. Generic analytical steady state phase diagram in the (Γ_b, b) plane with log-log scales for an $L1_2$ stoichiometric binary alloy irradiated at a temperature below its equilibrium order-disorder transition, T_c. "LRO" stands for long-range ordered steady state. The boundaries correspond to instability lines, from "Patterning" to "LRO," "Disordered" to "LRO," and "Disordered" to "Patterning." $\Gamma_{b,c}$ refers to the ballistic jump frequency at the "Disordered" to "LRO" transition, and b_c to the threshold cascade size for patterning to be possible.

the LRO state and the patterned state or the disordered state. This would require the use of global stability criteria,[8–10] a difficult task that is beyond the goal of the present work. We expect, and we will show in the next paragraph, that the instability lines constructed here offer already a very good prediction of the topology of the full dynamical phase diagram. In particular, not too close to a boundary in the diagram Fig. 1, the most stable steady states in the regions labeled "D," "LRO," and "P" are expected to be the disordered state, the long-range ordered state, and the state of patterning of order, respectively.

We now compare this analytical phase diagram to the one constructed in Part 1 from KMC results, i.e., Fig. 8 of Part 1. The two phase diagrams share a similar topology, with three distinct regions. We note that the existence of a minimum cascade size for the stabilization of patterns of order is not a prediction of the analytical model, but it is rather a direct consequence of the observation that a two-stage reordering is required for a possible stabilization of these patterns. Now regarding the patterning-LRO boundary, the remarkable result is that a power law with the $-3/2$ exponent predicted by Eq. (20) describes very well the KMC boundary. The second remarkable result is that the disorder-patterning instability line is only slightly shifted to lower Γ_b values as b increases. As stated in Sec. IV, mean field models using the Bragg-Williams approximation predict that this boundary should be vertical, i.e., only dependent of Γ_b. One published work relying on a pair approximation for the $A2$-$B2$ transition, however, predicts a finite suppression of the ballistic exchange frequency for the ordering instability in the large b limit, of about 15% at $T \approx 0.23 T_c$.[11] While this result cannot be directly transposed in a quantitative way to the present $A1$-$L1_2$ transition, it is consistent with the trend observed in the KMC diagram, Fig. 8 in Part 1: the instability line shifts from $\Gamma_b = 47.8\ s^{-1}$ for $b=1$ to $\Gamma_b = 17.9\ s^{-1}$ for $b=4002$. Despite the good qualitative agreement between the two phase diagrams, we did not attempt to compare them quantitatively for several reasons. First, for a given set of atomic interactions, the Bragg-Williams approximation is well known to largely overestimate the equilibrium order-disorder transition temperature, and to fail to reproduce the general topology of the composition-temperature phase diagram. Second, there are several unknown parameters in the equations derived here. The constant C_2 in Eqs. (17)–(20) depends on the exact geometry of the APBs. The constant ϕ, which links the average curvature to the specific APB area, is unknown, as well as the exact value of b_c. One may estimate or determine all these unknown quantities from the KMC simulations, but this approach would defeat the purpose of performing an independent quantitative test of the analytical phase diagram. It is nevertheless useful to estimate from the model the largest patterns of order that can be stabilized for a given cascade size. To that end we combine Eqs. (19) and (20), and we express S_v at the patterning-LRO transition in terms of the radius of the cascade size, r and of numerical constants:

$$S_v = \frac{5 \times 2^{1/3}}{4 \times 0.8} \cdot \frac{C_2}{1 + C_2} \cdot \frac{3}{r}. \tag{21}$$

We can estimate numerically S_v in the following way. If we assume that the microstructure is comprised of spherical domains of radius R_d, it follows that $S_v = 3/R_d$. We can then deduce from Eq. (21) that the maximum domain radius in the patterning regime is proportional to the cascade size. The exact proportionality constant between r and R_d is a function of C_2, which is itself a constant of the order of unity. When C_2 is of the order of unity, Eq. (21) yields $R_d \approx r/2$. On the other hand, an upper estimate for R_d is obtained by letting C_2 be large compared to one, which yields $R_d \approx r$. We can therefore conclude that the model predicts that the maximum size of the patterns of order is equal to the cascade size, multiplied by a geometrical factor close to unity. This result is fully consistent with the patterning mechanism discussed in the paper. As reviewed in the introduction, the cascade size ranges typically from a few to about 10 nm, and the patterns of order should therefore be at the same nanometer scale.

The present model can be directly generalized to other order-disorder phase transitions, at least when the ordering reaction can be described by a one-dimensional order parameter, e.g., the $A2$-$B2$ or the $A1$-$L1_0$ transitions. It is therefore expected that patterning of order under irradiation is a generic phenomenon. Nevertheless, one motivation for studying in detail the $A2$-$B2$ and the $A1$-$L1_0$ transitions is that the number of ordering variants in the $B2$ and $L1_0$ structures is 2 and 6, respectively. This could influence the connectivity of the domains in the patterning state, which could in turn affect the stability of this state. Finally, the KMC and analytical phase diagrams offer specific predictions that can be tested by carefully designed experiments, as discussed in Part 1. Besides testing the existence of the state of patterning of order, it would be particularly insightful to investigate whether there is a minimum cascade size for this patterning state to be stabilized under irradiation. In such experiments, the cascade size would be varied by adjusting the mass and the energy of the projectiles used for irradiation.[12]

VI. CONCLUSION

We have modeled the effect of the disordered zones introduced by displacement cascades on the evolution of the field of chemical order in a binary alloy under irradiation. Using a continuum description, we have derived a kinetic equation for the volume fraction of the various variants of an ordered structure. By combining this volume equation with the classical Allen-Cahn equation for the evolution of the antiphase area, we have identified a transition from a steady state that is locally ordered but lacks long-range order to a long-range ordered steady state. We have used this transition, as well as existing mean-field results for the ordering instability, to construct a dynamical steady-state phase diagram for a stoichiometric $L1_2$ alloy. From this analytical phase diagram, three possible steady states are expected, long-range ordered, disordered with some short-range order, and a state of patterning of order. The domain of stability of these three regions is in good agreement with a phase diagram built from KMC simulations. The analytical model predicts that the cascade size at the transition from long-range order to patterning of order scales as $(\Gamma_b)^{-3/2}$, which is in excellent agreement with the KMC results. Mean-field results in the Bragg-Williams approximation predict that the ordering instability boundary is a function of the disordering rate, Γ_b, but not of the cascade size *per se*. KMC results indicate that the ordering instability transition is in fact somewhat shifted to lower disordering rates as the cascade size increases, in agreement with a kinetic mean-field model based on a statistical approximation better than the point approximation. The present analytical treatment makes it possible to generalize the results obtained by KMC simulations in Part 1, and to propose that the dynamical stabilization of patterns of order is a general phenomenon under irradiation, as long as the disordered zones produced by the displacement cascades are large enough to result in the transient formation of antiphase domains during their thermal annealing.

ACKNOWLEDGMENTS

Stimulating exchanges with R. Holyst are gratefully acknowledged. This material is based upon work partly supported by the U.S. Department of Energy, Division of Materials Sciences under Award No. DEFG02-91ER45439, through the Frederick Seitz Materials Research Laboratory at the University of Illinois at Urbana-Champaign, by the Materials Computation Center at the University of Illinois, National Science Foundation, under Grants No. DMR 99-76550 and No. DMR 03-25939, and by the University of Illinois Campus Research Board.

*Electronic address: bellon@uiuc.edu

[1] J. Ye and P. Bellon, preceding paper, Phys. Rev. B **70**, 094104 (2004).

[2] S. M. Allen and J. W. Cahn, Acta Metall. **27**, 1085 (1979).

[3] D. Le Floc'h, P. Bellon, and M. Athenes, Phys. Rev. B **62**, 3142 (2000).

[4] M. Fialkowski, A. Aksimentiev, and R. Holyst, Phys. Rev. Lett. **86**, 240 (2001).

[5] M. Fialkowski and R. Holyst, Phys. Rev. E **66**, 046121 (2002).

[6] The distribution of local mean curvatures shown in Fig. 5 in Ref. 5 is well fitted by a Gaussian distribution, although other distributions based on a Lorentzian function could be used as well. The use of other distributions would only introduce a small numerical correction to the present equation.

[7] F. Ducastelle, *Order and Phase Stability in Alloys* (North-Holland, Amsterdam, 1991).

[8] P. Bellon and G. Martin, Phys. Rev. B **39**, 2403 (1989).

[9] P. Bellon and G. Martin, Phys. Rev. B **38**, 2570 (1988)

[10] F. Haider, P. Bellon, and G. Martin, Phys. Rev. B **42**, 8274 (1990).

[11] E. Salomons, P. Bellon, F. Soisson, and G. Martin, Phys. Rev. B **45**, 4582 (1992).

[12] R. S. Averback and T. Diaz de la Rubia, Solid State Phys. **51**, 281 (1998).